ELSEVIER

Contents lists available at ScienceDirect

## **Chemical Physics Letters**

journal homepage: www.elsevier.com/locate/cplett



#### Research paper



# A computational and experimental examination of the CID of phosphorylated serine-H<sup>+</sup>

George L. Barnes a,\*, Kristopher J. Kolonko b, Kenneth Lucas c,1, Klaudia A. Poplawski c

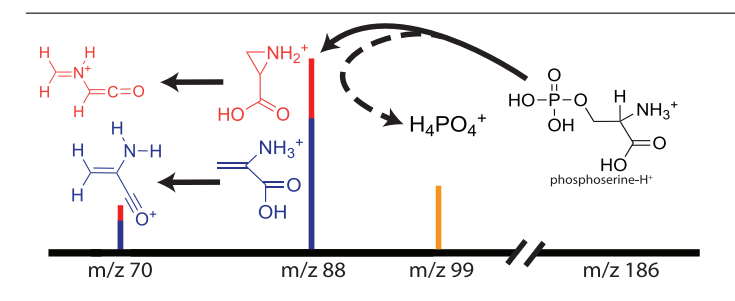
- <sup>a</sup> Department of Chemistry Illinois State University, Campus Box 4160 Normal, IL 61790-4160, United States of America
- b Stewart's Advanced Instrumentation and Technology (SAInT) Center Siena College, 515 Loudon Road, Loudonville, NY 12211, United States of America
- <sup>c</sup> Department of Chemistry and Biochemistry Siena College, 515 Loudon Road, Loudonville, NY 12211, United States of America

#### HIGHLIGHTS

#### First direct dynamics study of collisioninduced dissociation for a phosphorylated amino acid.

- Presents potential energy interaction parameters between argon and phosphorylated amino acids.
- Compares phosphorylation vs sulfonation of serine.

#### GRAPHICAL ABSTRACT



#### ARTICLE INFO

# Keywords: Collision induced dissociation Post-translational modification Direct dynamics simulation Graph theory

#### ABSTRACT

We present and discuss results from direct dynamics simulations, DFT calculations, and experimental measurements of the collision induced dissociation (CID) of O-phosphorylation of serine-H<sup>+</sup> (p-Ser, m/z186). Parameters for the interaction potential suitable for use in CID simulations of phosphorylated species were obtained and reported. Within both experiments and simulations, the primary decomposition product is m/z88. This agrees with previous studies, and simulations are consistent with the proposed primary mechanisms suggested in the literature for forming this product. Moreover, the simulations provided insight into an indirect decomposition pathway that forms m/z99 and secondary decomposition pathways observed experimentally at larger collision energies.

#### 1. Introduction

Post-translational modifications (PTMs) are common and expand the functionality of proteins [1–3]. However, they can also complicate protein investigations via tandem mass spectrometry, which is commonly used to study systems of biological interest [4–7]. Phosphorylation is a common PTM; the impacts of which on collision-induced dissociation (CID) has received considerable attention [8–14]. Phosphorylation is challenging from a tandem mass spectrometry point of view due to the lability of the phosphate group. In addition, the O-phosphorylation and O-sulfonation result in m/z values that require

high resolution to distinguish. Their CID decomposition pathways are also similar.

Direct dynamics simulations [15–21] and *ab initio* calculations have a history of providing significant and impactful insight into the dynamics taking place in tandem mass spectrometry. However, only a few systems that contain PTMs have been studied using these techniques. It can be challenging to undertake direct dynamics simulations since the parameters that define the interaction potential between the PTM and argon gas are required to simulate explicit argon CID. While the literature already provides the parameters needed to simulate the CID

E-mail address: glbarn3@ilstu.edu (G.L. Barnes).

<sup>\*</sup> Corresponding author.

<sup>&</sup>lt;sup>1</sup> Presently at SUNY Upstate Medical University; College of Medicine;766 Irving Avenue; Syracuse, NY 13210.

unmodified and sulfonated species, no previous study of a phosphorylated species exists. In this work, we report the necessary interaction parameters to perform direct dynamics simulations of phosphorylated species.

We use these new parameters to study the CID of the Ophosphorylation of serine (p-Ser). Both experimental and computational results are reported. Since we have previously examined the CID of the sulfonated analogue, s-Ser [17], comparisons between the two systems will be provided, where appropriate. p-Ser has been the focus of numerous experimental studies, and much work has been performed to elucidate the primary reaction mechanisms. Hence, this is a good test system for these new interaction parameters. Both p-Ser and s-Ser have the same nominal mass of m/z 186 and share a prominent CID peak at m/z 88 that results from the loss of the PTM as  $H_3PO_4$  and  $H_2SO_4$ , respectively. The literature has explored several potential mechanisms for this loss, with the two most prominent being direct loss via  $\beta$ elimination resulting in protonated 2-amino-propenoic acid and proton transfer from the N-terminus followed by SN2 nucleophilic attack on the  $\beta$  carbon to result in protonated 2-carboxy-aziridine. Both of these pathways will be discussed in greater detail below. It is noteworthy that while p-Ser and s-Ser share the m/z 88 peak, they do not have identical CID spectra across a range of collision energies. In particular, s-Ser has a significant population in m/z 106 (loss of  $SO_3$ ) and in m/z 140 (loss of  $H_2O + CO$ ). Both peaks have significantly smaller populations in p-Ser. At larger collision energies, experiments find that p-Ser has secondary decomposition products that have received less experimental focus. The reaction dynamics and structures of these species as revealed by simulations, are also reported. In addition, an indirect mechanism that leads to m/z 99 is seen in simulations.

An outline for the remainder of the paper is as follows: in Section 2, we provide an overview of our computational and experimental methods; in Section 3, we present our results; and in Section 4, we provide an overview.

#### 2. Methods

We have previously presented the results of both experimental and computational work on s-Ser. [17] We use the same general techniques for the p-Ser system, which are briefly outlined.

#### 2.1. Computational approach

Within this section, we briefly outline our computational approach. We refer the interested reader to the recent perspectives on this approach [15,19,22] and a tutorial review on the methods involved [19] for more details regarding the computational methods.

#### 2.1.1. Ar - PO<sub>4</sub> interaction potential

One method for performing direct dynamics simulations of CID involves modeling the collision between the inert gas argon and the system of interest. The typical approach models the interaction between the argon atom and the system as a sum of Buckingham two-body interactions, i.e.

$$V_{Ar,sys} = \sum_{i} A_{Ar,i} e^{(-B_{Ar,i} R_{Ar,i})} + \frac{C_{Ar,i}}{R_{Ar,i}^{9}}$$
(1)

where i runs over all atoms within the system of interest and  $R_{\rm Ar,i}$  is the distance between the argon and the ith atom of the system. The parameters A, B, and C depend on the chemical identity and environment of the ith atom. This form of interaction is purely repulsive in nature. The literature [23,24] provides these parameters for several different types of atoms, which were obtained by performing frozen potential energy scans of Ar interacting with small molecules with a similar chemical environment. It is common for these scans to select different orientations that emphasize specific limiting cases for the interactions. All of the ab initio electronic energies from each scan are

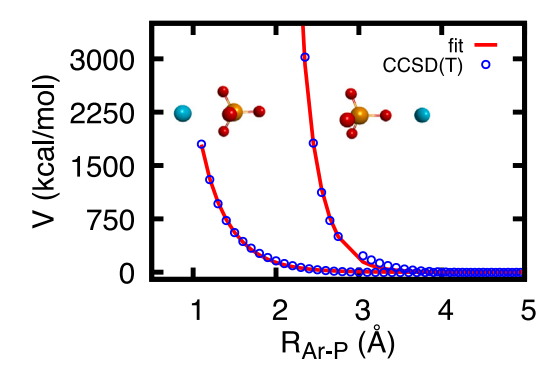


**Fig. 1.** A comparison of the CCSD(T) frozen potential scan and the fit to a sum of two-body Buckingham potentials. The fit simultaneously optimizes both orientations shown above and provides a good reproduction of the repulsive wall.

**Table 1** Parameters for the interaction between Ar and P=O with A, B, and C in kcal/mol,  $\mathring{A}^{-1}$ , and  $\mathring{A}^{9}$ kcal/mol, respectively.

Parameter type	A	В	С
Ar – O	56597.86	4.1803	21.200
Ar – P	31361.11	2.8223	450.930

simultaneously fit to obtain the parameters *A*, *B*, and *C*. Obtaining a good fit simultaneously for these limiting orientations provides confidence that the resulting interaction potential will yield good results for all orientations.

The literature does not currently provide parameters for Ar interacting with the phospho- PTM. As this is a common PTM that others may wish to simulate, here we undertake finding these parameters. The literature does provide potential terms for Ar interacting with OH groups, but new terms are needed for Ar interacting with the P atom and oxygen doubly bound to P. Hence, we report potential parameters for the Ar -  $PO_4^{3-}$  system suitable for CID calculations. Our frozen potential energy scans at the  $CCSD(T)/6-31++G^{**}$  level of theory and basis set were calculated for two orientations of the Ar - $PO_{\lambda}^{3-}$  system. The energy at each point was simultaneously fit using a genetic algorithm to a sum of two-body Buckingham potentials. A comparison of the ab initio CCSD(T) data and fit is depicted in Fig. 1 with the new potential parameters provided in Table 1. We note here that the ab initio data has a shallow attractive interaction present with a well depth of  $\sim -4.5$  kcal/mol. The functional form in Eq. (1) is purely repulsive and designed to reproduce the hard repulsive wall. So while these interaction parameters are suitable for the energy regime of CID simulations, they would not be appropriate for very low energy collisions in which association could occur.

### 2.1.2. Direct dynamics simulation method

With all of the "intermolecular" parameters for the Ar – p-Ser collision system in hand, we turn our attention to direct dynamics simulations. The initial structure of p-Ser was determined using Avogadro [25] with the phosphorylation occurring on the side-chain oxygen and the excess proton placed on the N-terminus. Direct dynamics simulations involving protonated peptides are commonly performed with PM6 [17,26] and the RM1 [16,21,22,26–29] semi-empirical methods. In our study of s-Ser, we found that PM6 outperformed RM1 [17], and expect similar results to be seen here. Hence, the initial structure generated via Avogadro's optimization routines was re-optimized using the PM6 semi-empirical method as implemented in Mopac2016 to yield the initial minimum energy structure [30].

Before starting a direct dynamics simulation, the initial conditions need to be defined. For each trajectory, the internal potential and kinetic energy of the p-Ser system were determined by sampling vibrational and rotational energy from a 300 K distribution via normal modes [31]. p-Ser was then placed 20 Å from the argon atom with a random orientation. The center of mass of p-Ser was then displaced by a randomly selected impact parameter with a maximum value of 3 Å. This maximum impact parameter resulted in a range of translational to internal energy transfers that sufficiently sampled chemical reactivity. The argon and p-Ser were then imparted a relative translational energy consistent with the selected collision energy. One thousand trajectories were calculated for relative collision energies of 3, 5, 7, 9, and 11 eV. As with the maximum impact parameter, these particular collision energies were selected to explore the products produced without producing too many low-mass species resulting from fast fragmentation events [18]. Final analysis was performed either as a function of collision energy or collectively for all collision energies considered depending on the question being answered. Generally speaking, reactivity increased with increasing collision energy.

The direct dynamics simulations themselves were propagated numerically by solving Hamilton's equations of motion using a 6th order symplectic integration scheme [32]. A maximum simulation time of 50 ps was calculated using a one fs step size and output written every 50 fs using our in-house simulation package tightly coupled with Mopac2012 [33] to calculate the p-Ser intramolecular potential energy using PM6 [34]. As we are focused on the charged fragments, neutral fragments were removed from the simulation if they were at least 15 Å away from any charged fragments. In addition, a trajectory was halted early if the final charged fragment had an  $m/z \leq 60$ . Conservation of energy was excellent for all trajectories.

#### 2.1.3. Theoretical mass spectra and reaction mechanisms

Our in-house simulation software provides the bond order between all QM atoms as a function of time throughout the simulation. A 5 fs window is used to average these bond orders to reduce momentary fluctuations resulting from vibrational motion. The averaged bond order matrix is converted to an adjacency matrix and saved every 50 fs. Postsimulation analysis is performed that identifies the simulation times when fragmentation occurs. Any such events that recombine within 100 fs are removed. Proton motion can be correlated to fragmentation times, allowing for an analysis of the influence of these migrations on dissociation events [35]. It was recently illustrated that this type of information could be combined with a graph theory analysis [16,36,37] to define a modified adjacency matrix weighted by the atomic number whose lowest eigenvalue is used to identify unique structures. Graph theory and direct dynamics provide powerful tools for analyzing reaction mechanisms. With the important structures identified using these tools, the energetics are obtained at the ωB97X-D/aug-cc-pVTZ level of theory as implemented in the Gaussian16 software package [38]. We note that many of the mechanisms described here are similar to those seen in s-Ser and were characterized at the same level in our previous work [16].

#### 2.2. Experimental approach

All chemicals were purchased from Sigma Aldrich and used without further purification. Samples were prepared in mass spectrometry-grade solvents containing a 1:1 mixture of acetonitrile and water. High-resolution mass spectrometry data were acquired on an unmodified Bruker Maxis Impact HD (Quadrupole-Time of Flight) spectrometer using sodium formate solution as the mass calibrant and the standard heated electrospray ionization (ESI) source. Pseudo-MS3 experiments were performed utilizing in-source fragmentation. Typical laboratory collision energies considered were 5, 10, 12.5, 15, 17.5, 20, 22.5, 25, 30, and 35 eV using nitrogen within the CID cell at a pressure of  $\sim 1\times 10^{-2}$  mbar based on Bruker's specifications.

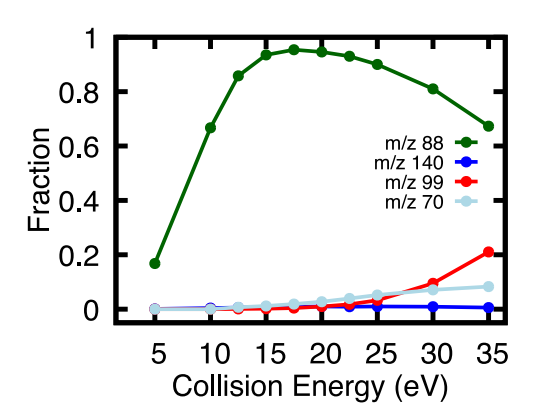


Fig. 2. The collision energy dependence of the major peaks observed experimentally. The reactant ion, m/z 186, is not shown for clarity, but has significant population at 5 and 10 eV but quickly approaches zero normalized intensity as m/z 88 becomes the major species present. At higher collision energies, additional products also start to be observed

Table 2 Energetics of the various exit channels in kJ/mol calculated at the  $\omega$ B97X-D/aug-cc-pVTZ level of theory.

m/z	Exit channel (kJ/mol)	
168 <sup>a</sup>	136.9	
140 <sup>b</sup>	192.2	
99 <sup>c</sup>	156.1	
88 (pathway 1)	137.2	
88 (pathway 2)	181.7	
70 (structure 3)	312.1	
70 (structure 4)	324.4	

<sup>&</sup>lt;sup>a</sup>H<sub>2</sub>O loss from side-chain.

#### 3. Results and discussion

The experimental measurements of p-Ser are summarized in Fig. 2, which presents the normalized intensity for several nominal m/z product peaks as a function of collision energy. m/z 88 is the only significant product at low to mid collision energies. As the collision energy increases, secondary and indirect fragmentation products begin to have larger populations, but m/z 88 is still the most significant peak. Examining the simulations and subsequent DFT calculations provides insight into these peaks.

Fig. 3 provides an example of the simulated mass spectra and the collision energy dependence of several peaks, while Table 2 provides a summary of energies of the various exit channels at the  $\omega$ B97X-D/aug-cc-pVTZ level of theory. The simulations agree with experiment in that at low collision energies m/z 88 is the primary product. However, we do note here that the total reactivity observed within the simulations is significantly less than that in experiment, primarily due to the time scale of the simulations and potentially the amount of energy transferred in the single collision event that was simulated. Moreover, the collision energy range considered is smaller for the simulations to avoid a significant increase in the population of peaks less than m/z 50, which our experimental measurements cannot observe.

#### 3.1. m/z 88: Loss of H<sub>3</sub>PO<sub>4</sub>

The loss of  $\rm H_3PO_4$  to yield m/z 88 is the most common product observed in simulations for most collision energies and corresponds to the loss of the side-chain PTM. This decomposition product was also

<sup>&</sup>lt;sup>b</sup>H<sub>2</sub>O loss (C-terminus) + CO

<sup>&</sup>lt;sup>c</sup>Indirect pathway involving an intermediate complex.

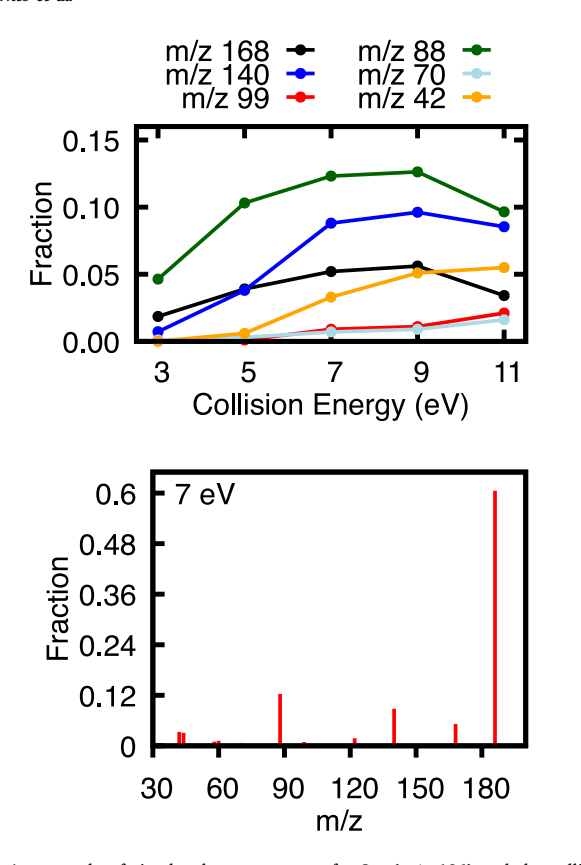


**Fig. 3.** An example of simulated mass spectra of p-Ser (m/z 186) and the collision energy dependence of notable peaks within simulations. The most commonly observed peak within the simulations is m/z 88, which corresponds to the loss of  $H_3PO_4$ , i.e., the modified side-chain. As collision energy increases, m/z 140 - loss of  $H_2O$  + CO - becomes more common.

the most common in our previous work on s-Ser. [17] The mechanisms described here for p-Ser are direct analogues to those outlined for s-Ser. Formation of m/z 88 is also the most dominant peak in experiments at moderate collision energies. This peak has received significant attention within the literature [8–14], with multiple proposed mechanisms suggested based on experimental evidence. This evidence indicates that an SN2 mechanism is likely, which will be described below.

Examining the simulation results shows that there are two major products associated with the m/z 88 peak. The most common pathway observed in simulations is a direct loss of  $\rm H_3PO_4$  initiated via a proton transfer from the  $\alpha$ -carbon to the oxygen of the phosphoryl group on the side chain. This results in protonated 2-amino propenoic acid (Structure 1) as the charged product, and is illustrated in scheme 1:

Our DFT calculations show that this exit channel is  $\sim 137.2 \text{ kJ/mol}$  higher in energy relative to the starting structure, i.e., N-protonated p-Ser. All DFT energies that we report define N-protonated p-Ser as the energy zero. Experimental works in the literature have previously proposed the mechanism in Scheme (1) for both p-Ser and its analogue in s-Ser; however, the most recent experimental works suggest that it is not the primary mechanism [9,11,13].

The second mechanism involves an initial transfer of a proton from the N-terminus to the oxygen of the P=O group on the side chain. Our DFT calculations show that it is energetically more favorable to place the hydrogen on the N-terminus, meaning that unless a conformational change accompanies this transfer, the proton would readily transfer back to the N-terminus. However, if a conformational change does occur, there is a stable minimum energy structure located at  $\sim 39.9\,$  kJ/mol above the global energy minimum. The simulations show a frequent change in the association between these two protonation sites. However, due to the strong hydrogen bonding present, there is no clearly defined transition state between these protonation states. Once the proton is located on the phosphate group, the N-terminus attacks the first carbon of the side-chain to induce the loss of  $\rm H_3PO_4$  and results in N-protonated 2-carboxy-aziridine (Structure 2), as illustrated in scheme 2:.

OH  

$$H_2N$$
OH
 $H_3PO_4 loss$ 
 $+H_2N$ 
OH
 $Protonated$ 
 $2-carboxy-aziridine$ 
(Structure 2)

DFT calculations show that this exit channel is at  $\sim 181.7~kJ/mol$  relative to N-protonated p-Ser. Based on experimental evidence reported in the literature, this SN2 mechanism is thought to be the dominant product formed in both p-Ser and s-Ser CID experiments [9,11,13].

Examining our simulations and considering all collision energies, the branching ratio between these two pathways is 0.81 (pathway 1) vs. 0.13 (pathway 2). Our DFT simulations find that the branched protonated 2-amino propenoic acid (Structure 1) is lower in energy than the cyclic N-protonated 2-carboxy-aziridine (Structure 2) by  $\sim$  44 kJ/mol. That said, the experimental work of both Lanucara et al. [9] and Reid et al. [14] provide evidence that pathway 2 is preferred. The simulations likely predict a qualitatively incorrect branching ratio between these products because the semi-empirical PM6 method, which is employed in the chemical dynamics simulations, predicts both a lower exit energy for pathway 1 and a higher exit energy for pathway 2 than seen in the DFT calculations. With this information in mind, it is not surprising that PM6 based simulations struggle to agree with the experimental preference.

Our graph theory analysis shows that these two structures account for a population fraction of 0.94 out of 1 within the peak. N-protonated 2-iminopropanoic acid accounts for an additional fraction of 0.04. Although this product is not commonly observed within simulations, at the DFT level, it has the lowest energy at  $\sim 120.4~\rm kJ/mol$  and could directly convert from Structure 1 via a hydrogen shift. The remaining population fraction - 0.02 - is found in eight uncommonly occurring structures that are unlikely to be stable on the time scale of the experiments and are transient intermediates captured at the end of the simulation time window.

#### 3.2. Formation of m/z 99, 70, 60, and 42

While the major focus of the literature has been on the formation of m/z 88, some works have noted other experimental peaks [9]. As seen in Figs. 2 and 3, our experimental and simulated spectra contain some other peaks. Both m/z 99 and 70 are related to structures formed from m/z 88. The formation of  $H_4PO_4^+$ , which corresponds to m/z 99, and its relation to m/z 88 is described below, while m/z 70 results from loss of water from m/z 88.

Our simulations indicate that the dominant means of forming  $H_4PO_4^+$  is via a continuation of the m/z 88 pathways described above, in which the  $H_3PO_4$  group does not immediately "leave" but rather forms a short-lived complex with the m/z 88 product. The  $H_3PO_4$  species can then abstract a proton from either the N-terminus or the former side-chains  $CH_2$  group. Forming  $H_4PO_4^+$  depends on either fast proton abstraction occurring or low translational energy, which allows for the formation of a complex. This species can form from either Structure 1 or 2. That said, the exit channel starting from Structure 1 is significantly

$$\begin{array}{c}
H & H \\
\longrightarrow N^{+} \\
H & \longrightarrow C = O \\
H \\
(Structure 3)
\end{array}$$

**Fig. 4.** The two m/z 70 structures formed from the loss of water from m/z 88. Structure 3 is predominately formed from protonated 2-carboxy-aziridine (Structure 2) and Structure 4 from protonated 2-amino propenoic acid (Structure 1) via water loss.

lower in final energy at 156.1 kJ/mol vs. 217.3 kJ/mol for Structure **2**. m/z 99 is a minor peak within the simulations that is also seen experimentally. Our experiments show that for most collision energies, it has a low population, but at 35 eV, m/z 99 has a relative population fraction of 0.21. Formation of m/z 99 via an intermediate complex between initial decomposition products is striking. Similar fragmentation dynamics involving complex formation have been observed previously in the literature, most recently by Macaluso and co-workers [26] who have termed this a "roaming" mechanism. It was also seen in simulations of the CID of urea [39], and our groups previous work on octaglycine [40].

m/z 70 is a decomposition product of m/z 88 that is seen in experiment and has a population of ~ 0.08 at a collision energy of 35 eV. The simulations predict two stable structures for this peak, Structures 3 and 4 which are shown in Fig. 4. The Structure 3 is predominately formed from N-protonated 2-carboxy-aziridine (Structure 2). This secondary process begins with the abstraction of a proton from the N-terminus by the carbonyl of the C-terminus. This transfer eventually results in ring opening and water loss. These two steps can happen nearly simultaneously or in a step-wise fashion. Structure 4 is predominately formed via water loss from Structure 1 via N- to C-terminus hydrogen transfer. In our simulations, Structure 3 makes up the majority of the peak at low collision energies. At large collision energies, Structure 4 is most common. When considering all collision energies, Structure 3 is the most commonly observed, with a branching ratio between these two products of 0.86 to 0.10. That said, given the small population of this peak in the simulations, this may not be statistically meaningful. The remaining population within the peak is identified as intermediates that would result in one of the two structures in Fig. 4 given enough simulation time. In simulations, m/z 42 is formed through two different pathways, one of which is the further water loss from m/z 70, and is the primary pathway observed. m/z 42 can also be formed by loss of  $H_3PO_4$  from m/z 140, which is discussed below.

Our previous simulations on unmodified serine found that the primary decomposition product was m/z 60. This peak is also present in the theoretical p-Ser mass spectrum and increases with increased collision energy. While there is some diversity in how this peak forms, it is seen that one of the primary means is through an initial loss of HPO $_3$  to regenerate N-protonated serine. This intermediate subsequently losses  $\rm H_2O+CO$  to form N-protonated 2-Iminoethanol.

#### 3.3. Formation of m/z 168 and 140

The peaks at m/z 168 and 140 represent a distinct reaction pathway from that of m/z 88 and correspond to the loss of water, and loss of water and CO, respectively. Neither represents major peaks in experiment, but m/z 140 is observed with a normalized intensity of at most  $\sim$  1%. Although one might expect to find that m/z 168 is an intermediate for m/z 140, and that can occur; in fact, the simulated m/z 168 peak most commonly arises from the loss of water from the phosphate group due to N-terminus attack on the P to form a five-membered ring structure. In contrast, m/z 140 most commonly occurs via the loss of the C-terminus. While m/z 140 is seen in our experimental measurements, m/z 168 is not.

Since the simulations overestimate both of these peaks compared to the experiment, we wished to ensure that this was not indicative of a deficiency in the new CID interaction parameters we reported here. Hence, additional simulations were performed using internal energy excitation rather than a direct collision event with argon. The internal energy was set to 606.7 kJ/mol, which is the average energy transferred to internal degrees of freedom following a collision with argon at 7 eV. Both m/z 140 and 168 are seen in these simulations with a significant population. This suggests that the interaction parameters are not at fault, but rather the semi-empirical method itself results in an overestimate of these pathways. This deficiency is more noticeable in p-Ser than in s-Ser given that the m/z 140 path has significant population as reported in the experimental work of by Polfer and coworkers [41]. Hence, it was not out of place to see this peak in the s-Ser simulations [17]. This observation suggests that the loss of the PTM is preferred significantly over the loss of the C-terminus in p-Ser and results in a dramatic reduction the experimentally observed population of m/z 140 compared to s-Ser.

#### 4. Summary

This work represents the first simulations of the phosphorylation post-translational modification, and we have reported potential energy interaction parameters suitable for future argon CID simulations that are based on high-level CCSD(T)/6-31++ $G^{**}$  ab initio calculations. These interactions were fit to two-body Buckingham parameters using a genetic algorithm and focus on reproducing the repulsive wall of the interaction.

Our simulations recover the major experimental decomposition product, namely loss of  $\rm H_3PO_4$ . The mechanisms observed in simulations are consistent with those previously proposed. It is accepted that the SN2 mechanism is likely the dominant pathway in experiment, while our simulations show the  $\beta$  elimination pathway as the primary mechanism. This is likely due to the energetics of the semi-empirical method used.

Secondary decomposition products are seen in both simulations and experiments. m/z 70 is seen experimentally and can be attributed to water loss from the primary m/z 88 peak. Two stable structures are seen in simulations for this peak, one for each of the most common structures within the m/z 88 peak. m/z 42, which has also been observed in previous experimental work, was seen in our simulations and results from loss of water from m/z 70. In addition to these secondary decomposition products, simulations show that  $H_4PO_4$  (m/z 99) can result from an indirect mechanism in which an intermediate complex is formed between  $H_3PO_4$  and the primary m/z 88 decomposition product. A proton transfer from m/z 88 to  $H_3PO_4$  then results in m/z 99.

In contrast to s-Ser, m/z 140 - loss of  $\rm H_2O + \rm CO$  - is not a common product observed in experimental work. However, this peak is observed in the present simulations and our previous work on s-Ser. The presence of m/z 140 is likely not a deficiency of the new CID interaction parameters but likely due to the semi-empirical method used for the direct dynamics simulations. It is interesting that s-Ser and p-Ser display a qualitative difference between their CID spectra.

#### CRediT authorship contribution statement

George L. Barnes: Conceptualization, Software, Investigation, Writing. Kristopher J. Kolonko: Investigation, Writing. Kenneth Lucas: Investigation. Klaudia A. Poplawski: Investigation.

#### Declaration of competing interest

The authors declare the following financial interests/personal relationships which may be considered as potential competing interests: George L. Barnes reports financial support was provided by National Science Foundation.

#### Data availability

Data will be made available on request.

#### Acknowledgments

The authors acknowledge the generous support from the National Science Foundation under Grant No. 1763652 and 2301606. GLB is a member of the MERCURY consortium, which receives support through National Science Foundation grant No. CHE-2018427.

#### References

- A. Kumar, V. Narayanan, A. Sekhar, Characterizing post-translational modifications and their effects on protein conformation using nmr spectroscopy, Biochemistry 59 (2020) 57–73, http://dx.doi.org/10.1021/acs.biochem.9b00827.
- [2] H. Ryšlavá, V. Doubnerová, D. Kavan, O. Vaněk, Effect of posttranslational modifications on enzyme function and assembly, J. Proteom. 92 (2013) 80–109, http://dx.doi.org/10.1016/j.jprot.2013.03.025.
- [3] C. Boscher, J.W. Dennis, I.R. Nabi, Glycosylation, galectins and cellular signaling, Curr. Opin. Cell Biol. 23 (2011) 383–392, http://dx.doi.org/10.1016/j.ceb.2011. 05.001.
- [4] R.G. Cooks, T. Ast, T. Pradeep, V.H. Wysocki, Reactions of ions with organic surfaces, Acc. Chem. Res. 27 (1994) 316–323, http://dx.doi.org/10.1021/ar00047a001.
- [5] I.A. Papayannopoulos, The interpretation of collision-induced dissociation tandem mass spectra of peptides, Mass Spectrom. Rev. 14 (1995) 49–73, http://dx.doi.org/10.1002/mas.1280140104.
- [6] E.R. Williams, Tandem ftms of large biomolecules, Anal. Chem. 70 (1998) 179A–185A, http://dx.doi.org/10.1021/ac981773x.
- [7] V.H. Wysocki, K.E. Joyce, C.M. Jones, R.L. Beardsley, Surface-induced dissociation of small molecules, peptides, and non-covalent protein complexes, J. Am. Soc. Mass Spectrom. 19 (2008) 190–208, http://dx.doi.org/10.1016/j.jasms. 2007.11.005
- [8] C.M. Potel, S. Lemeer, A.J. Heck, Phosphopeptide fragmentation and site localization by mass spectrometry: An update, Anal. Chem. 91 (2019) 126–141, http://dx.doi.org/10.1021/acs.analchem.8b04746.
- [9] F. Lanucara, B. Chiavarino, D. Scuderi, P. Maitre, S. Fornarini, M.E. Crestoni, Kinetic control in the cid-induced elimination of H<sub>3</sub>PO<sub>4</sub> from phosphorylated serine probed using irmpd spectroscopy, Chem. Commun. 50 (2014) 3845–3848, http://dx.doi.org/10.1039/C4CC00877D.
- [10] J. Laskin, R.P. Kong, T. Song, I.K. Chu, Effect of the basic residue on the energetics and dynamics of dissociation of phosphopeptides, Int. J. Mass Spectrom. (2012) 295–301, http://dx.doi.org/10.1016/j.ijms.2012.09.013.
- [11] M. Rožman, Modelling of the gas-phase phosphate group loss and rearrangement in phosphorylated peptides, J. Mass Spectrom. 330–332 (2011) 949–955, http: //dx.doi.org/10.1002/JMS.1974.
- [12] P.J. Boersema, S. Mohammed, A.J. Heck, Phosphopeptide fragmentation and analysis by mass spectrometry, J. Mass Spectrom. 44 (2009) 861–878, http: //dx.doi.org/10.1002/JMS.1599.
- [13] A.M. Palumbo, J.J. Tepe, G.E. Reid, Mechanistic insights into the multistage gas-phase fragmentation behavior of phosphoserine- and phosphothreoninecontaining peptides, J. Proteome Res. 7 (2008) 771–779, http://dx.doi.org/10. 1021/PR0705136/SUPPL\_FILE/PR0705136-FILE006.PDF.
- [14] G.E. Reid, R.J. Simpson, R.A. O'Hair, Leaving group and gas phase neighboring group effects in the side chain losses from protonated serine and its derivatives, J. Am. Soc. Mass Spectrom. 11 (2000) 1047–1060, http://dx.doi.org/10.1016/ \$1044-0305(00)00189-6.
- [15] A.M. Somer, V. Macaluso, G.L. Barnes, L. Yang, S. Pratihar, K. Song, W.L. Hase, R. Spezia, Role of chemical dynamics simulations in mass spectrometry studies of collision-induced dissociation and collisions of biological ions with organic surfaces, J. Am. Soc. Mass Spectrom. 31 (2020) 2–24, http://dx.doi.org/10.1021/ jasms.9b00062.

- [16] K. Lucas, A. Chen, M. Schubmehl, K.J. Kolonko, G.L. Barnes, Exploring the effects of methylation on the cid of protonated lysine: A combined experimental and computational approach, J. Am. Soc. Mass Spectrom. 32 (2021) 2675–2684, http://dx.doi.org/10.1021/jasms.1c00225.
- [17] K. Lucas, G.L. Barnes, Modeling the effects of o-sulfonation on the cid of serine, J. Am. Soc. Mass Spectrom. 31 (2020) 1114–1122, http://dx.doi.org/10.1021/jasms.0c00037.
- [18] G.L. Barnes, A. Shlaferman, M. Strain, Fast fragmentation during surface-induced dissociation: An examination of peptide size and structure, Chem. Phys. Lett. 754 (2020) 137716, http://dx.doi.org/10.1016/j.cplett.2020.137716.
- [19] S. Pratihar, G.L. Barnes, W.L. Hase, S. Pratihara, G.L. Barnes, W.L. Hase, Chemical dynamics simulations of energy transfer, surface-induced dissociation, soft-landing, and reactive- landing in collisions of protonated peptide ions with organic surfaces, Chem. Soc. Rev. 45 (2016) 3595–3608, http://dx.doi.org/10. 1039/C5CS00482A.
- [20] S. Pratihar, G.L. Barnes, J. Laskin, W.L. Hase, Dynamics of protonated peptide ion collisions with organic surfaces. Consonance of simulation and experiment, J. Phys. Chem. Lett. 7 (2016) 3142–3150, http://dx.doi.org/10.1021/acs.jpclett. 6b00978.
- [21] D. Frederickson, M. McDonough, G.L. Barnes, A computational comparison of soft landing of alpha-helical vs globular peptides, J. Phys. Chem. B 122 (2018) 9549–9554, http://dx.doi.org/10.1021/acs.jpcb.8b06232.
- [22] G.L. Barnes, W.L. Hase, Energy transfer, unfolding, and fragmentation dynamics in collisions of N-protonated octaglycine with an h-sam surface, J. Am. Chem. Soc. 131 (2009) 17185–17193, http://dx.doi.org/10.1021/ja904925p.
- [23] O. Meroueh, W.L. Hase, Collisional activation of small peptides, J. Phys. Chem. A 103 (1999) 3981–3990, http://dx.doi.org/10.1021/jp984712b.
- [24] D. Ortiz, J.-Y. Salpin, K. Song, R. Spezia, Galactose-6-sulfate collision induced dissociation using QM+MM chemical dynamics simulations and esi-ms/ms experiments, Int. J. Mass Spectrom. 358 (2014) 25–35, http://dx.doi.org/10.1016/ i.iims.2013.11.002.
- [25] M.D. Hanwell, D.E. Curtis, D.C. Lonie, T. Vandermeersch, E. Zurek, G.R. Hutchison, Avogadro: An advanced semantic chemical editor, visualization, and analysis platform, J. Cheminformatics 4 (2012) 17, http://dx.doi.org/10.1186/1758-2946-4-17.
- [26] V. Macaluso, D. Scuderi, M.E. Crestoni, S. Fornarini, D. Corinti, E. Dalloz, E. Martinez-Nunez, W.L. Hase, R. Spezia, L -cysteine modified by s-sulfation: Consequence on fragmentation processes elucidated by tandem mass spectrometry and chemical dynamics simulations, J. Phys. Chem. A 123 (2019) 3685–3696, http://dx.doi.org/10.1021/acs.jpca.9b01779.
- [27] G.L. Barnes, K. Young, L. Yang, W.L. Hase, Fragmentation and reactivity in collisions of protonated diglycine with chemically modified perfluorinated alkylthiolate-self-assembled monolayer surfaces, J. Chem. Phys. 134 (2011) 094106, http://dx.doi.org/10.1063/1.3558736.
- [28] Z. Homayoon, S. Pratihar, E. Dratz, R. Snider, R. Spezia, G.L. Barnes, V. Macaluso, A.M. Somer, W.L. Hase, Model simulations of the thermal dissociation of the TIK(H<sup>+</sup>)<sub>2</sub>tripeptide: Mechanisms and kinetic parameters, J. Phys. Chem. A 120 (2016) 8211–8227, http://dx.doi.org/10.1021/acs.jpca.6b05884.
- [29] M. Gu, J. Zhang, W.L. Hase, L. Yang, Direct dynamics simulations of the thermal fragmentation of a protonated peptide containing arginine, ACS Omega 5 (2020) 1463–1471, http://dx.doi.org/10.1021/acsomega.9b03091.
- [30] J.P. Stewart, Mopac2016, 2016.
- [31] G.H. Peslherbe, H. Wang, W.L. Hase, Monte Carlo sampling for classical trajectory simulations, Adv. Chem. Phys. 105 (1999) 171–201, http://dx.doi.org/10.1002/9780470141649.
- [32] C. Schlier, A. Seiter, High-order symplectic integration: An assessment, Comput. Phys. Comm. 130 (2000) 176–189, http://dx.doi.org/10.1016/S0010-4655(00) 00011-4.
- [33] J.P. Stewart, Mopac2012, 2012.
- [34] J.J.P. Stewart, Optimization of parameters for semiempirical methods V: modification of nddo approximations and application to 70 elements, J. Mol. Model. 13 (2007) 1173–1213, http://dx.doi.org/10.1007/s00894-007-0233-4.
- [35] Z. Gregg, W. Ijaz, S. Jannetti, G.L. Barnes, The role of proton transfer in surface-induced dissociation, J. Phys. Chem. C 118 (2014) 22149–22155, http://dx.doi.org/10.1021/jp507069x.
- [36] S.A. Vázquez, X.L. Otero, E. Martinez-Nunez, A trajectory-based method to explore reaction mechanisms, Molecules 23 (2018) 3156, http://dx.doi.org/10. 3390/molecules23123156.
- [37] A. Rodríguez, R. Rodríguez-Fernández, S.A. Vázquez, G.L. Barnes, J.J.P. Stewart, E. Martínez-Núñez, tsscds2018: A code for automated discovery of chemical reaction mechanisms and solving the kinetics, J. Comput. Chem. 39 (2018) 1922–1930, http://dx.doi.org/10.1002/jcc.25370.
- [38] M.J. Frisch, G.W. Trucks, H.B. Schlegel, G.E. Scuseria, M.A. Robb, J.R. Cheeseman, G. Scalmani, V. Barone, G.A. Petersson, H. Nakatsuji, X. Li, M. Caricato, A.V. Marenich, J. Bloino, B.G. Janesko, R. Gomperts, B. Mennucci, H.P. Hratchian, J.V. Ortiz, A.F. Izmaylov, J.L. Sonnenberg, D. Williams-Young, F. Ding, F. Lipparini, F. Egidi, J. Goings, B. Peng, A. Petrone, T. Henderson, D. Ranasinghe, V.G. Zakrzewski, J. Gao, N. Rega, G. Zheng, W. Liang, M. Hada, M. Ehara, K. Toyota, R. Fukuda, J. Hasegawa, M. Ishida, T. Nakajima, Y. Honda, O. Kitao, H. Nakai, T. Vreven, K. Throssell, J.A.M. Jr., J.E. Peralta, F. Ogliaro, M.J.

- Bearpark, J.J. Heyd, E.N. Brothers, K.N. Kudin, V.N. Staroverov, T.A. Keith, R. Kobayashi, J. Normand, K. Raghavachari, A.P. Rendell, J.C. Burant, S.S. Iyengar, J. Tomasi, M. Cossi, J.M. Millam, M. Klene, C. Adamo, R. Cammi, J.W. Ochterski, R.L. Martin, K. Morokuma, O. Farkas, J.B. Foresman, D.J. Fox, Gaussian 16 Revision C.01, gaussian Inc., Wallingford CT, 2016.
- [39] R. Spezia, J.-Y. Salpin, M.-P. Gaigeot, W.L. Hase, K. Song, Protonated urea collision-induced dissociation. Comparison of experiments and chemical dynamics simulations, J. Phys. Chem. A 113 (50) (2009) 13853–13862, http://dx.doi. org/10.1021/jp906482v.
- [40] W. Ijaz, Z. Gregg, G.L. Barnes, Complex formation during sid and its effect on proton mobility, J. Phys. Chem. Lett. 4 (2013) 3935–3939, http://dx.doi.org/10. 1021/jz402093a.
- [41] A.L. Patrick, C.N. Stedwell, B. Schindler, I. Compagnon, G. Berden, J. Oomens, N.C. Polfer, Insights into the fragmentation pathways of gas-phase protonated sulfoserine, Int. J. Mass Spectrom. (2014) http://dx.doi.org/10.1016/j.ijms.2014. 12.001.